PiscoMed Publishing

doi: 10.18282/i-es.v6i1.568

Review article

Fundamentals of different wind turbines for electricity generation and their modelling methods using different algorithms

Ranjbar Zohreh[1], Shahab Jalili Sheshbahreh[2], Mahsa Ghorbani[3], Rahim Zahedi[4], Mansour Keshavarzzadeh[5], Hossein Yousefi[4,*]

[1] Department of Computer Engineering and Information Technology, Qazvin Islamic Azad University, Qazvin 45617, Iran

[2] Faculty of Electrical Engineering, Amirkabir University of Technology, Tehran 11369, Iran

[3] Department of Civil Engineering, Amirkabir University of Technology, Tehran 11369, Iran

[4] Department of Renewable Energy and Environmental Engineering, University of Tehran, Tehran 11369, Iran

[5] Faculty of Mechanical Engineering, Iran University of Science and Technology, Tehran 11369, Iran

*** Correspond author:** Hossein Yousefi, hosseinyousefi@ut.ac.ir

Abstract: Increased concern for the environment has led to the search for more environment-friendly energy sources so that wind energy can be used as an endless option for human consumption. Wind turbines offer a promising solution for off-grid areas. However, they have certain drawbacks associated with different configurations. Darrieus turbine is one type that can be more efficient than other types. The poor start-up performance of Darrieus turbines is one of the critical problems restricting its development. Another problem of this kind of wind turbine is tackled by identifying the optimization parameters, such as complex flow dynamics around the system. The present article reviews modeling vertical axis turbines methods and discusses the turbine's operation by presenting the results of these methods. In this review, the authors have attempted to compile the main aerodynamic models that have been used for performance prediction and design of straight-bladed Darrieus-type VAWT. The main object of this study is to research the advantages and disadvantages of wind turbine modeling methods, and the selection of these methods depends on the purpose of the modeling.

Keywords: particle image velocimetry; darrieus; wind turbine; aerodynamics; CFD; modeling

Received: 26 February 2023; **Accepted**: 22 May 2023; **Available online**: 30 August 2023

1. Introduction

The focus on renewable energy sources has increased significantly in recent years due to environmental pollution, increasing energy demand, and declining fossil fuel resources. Various sources of renewable energy include biomass[1], solar[2], geothermal[3], hydroelectric[4], and wind[5,6]. In the meantime, the wind has been proven to be a cheaper alternative to energy, and hence extensive research efforts have been made to improve wind power generation technology[7,8]. The world has enormous potential for wind energy that can be used to generate electricity. According to research by Iran's New Energies Organization, Iran has areas with good potential for wind energy. Since wind speed is different in different parts of the country, a suitable turbine must be selected with environmental conditions to efficiently use wind energy to have a proper economic justification[9–11].

Over the past ten years, electricity generation capacity has increased from 25 GW to 200 GW for the

vertical axis wind turbines[12]. The first type of manufactured wind turbine might be a drag-type vertical axis wind turbine (VAWT) used in the Sistan region[13–16]. Although VAWTs were the first turbines used by humans, modern-day researchers have shown more interest in them because they can generate electricity on a large scale. In recent decades, horizontal axis wind turbines (HAWTs) have been extensively researched, and the vast majority of the installed capacity of wind turbines is related to this type of turbine[17–19].

However, research on VAWT continued in parallel on a smaller scale. Solving the main problems related to VAWTs, such as blade lift force, blade failure due to oscillating force and wind, etc.[20–22], are some common previous studies, but more research is needed. VAWTs currently need to be more economically attractive on a large scale[13,23,24]. However, VAWT is a way to generate energy in locations away from the main distribution line or where wind farms cannot be used due to environmental issues, so small-scale dispersed generation units are preferred[25,26]. For the reason of negative environmental impacts and the distance of these turbines from distribution lines, mass production of VAWTs has only recently begun as a small-scale production unit and not as a large commercial wind farms yet[27–29].

Scientists, especially Darrieus and Savonius, have created various configurations of this type of turbine and used different methods for their studies[16,30]. This paper examines the details of techniques and configurations, along with researchers' crucial findings about VAWTs. A new method for investigating this turbine type will be proposed and compared with previous samples. Also, the table of the abbreviations is attached as the supplementary materials to this manuscript.

2. Wind turbines configuration

Differences in the shape and efficiency of wind turbines cause differences in the appropriate conditions of their use. In this section, we will review the types of turbines and compare them.

2.1. HAWTs

The first electrical-producing wind turbines were Scottish, Danish, French, and American[21], and the Brush turbine was built in 1888[20,31]. Nevertheless, modern VAWTs (**Figure 1**), used commercially for wind farms to generate electricity, usually have three blades that provide the force needed to rotate the rotor by lift force. The blades are positioned in the wind direction by a computer-controlled motor. At the top of the tower is a gearbox and a generator, and the blades are connected to this part. These turbines have been a significant part of the contemporary history of wind energy technology and are a standard commercial type. Although the efficiency of these turbines is high[32–34], it also has disadvantages that will be mentioned in the next section.

2.2. Drag-type VAWTs

Sistan wind turbine, the first type of wind turbine, falls into this category. However, the most famous type of this category, which has a higher efficiency than other cases of drag type, is the Savonius rotor, whose name is derived from the name of its Finnish designer. This type of turbine, a drag-type and vertical axis, were first tested in 1925. This rotor was very popular in the 1960s and 1970s due to its simple construction and production, high starting torque, and ability to accept wind force from all directions. However, it has some disadvantages, such as high weight, low efficiency (15%–19%), high torque changes on the axis of rotation, and wind from low latitudes, which made it out of the spotlight over time made[35–37].

The mechanism of this type of turbine is such that the wind drag force in the concave part of the turbine is more than the convex part, and therefore it will cause the rotor to rotate[38]. After passing through the concave part, the fluid enters the other half of the rotor to apply a force against wind flow and in the

direction of rotation. Regardless of the drag force in the convex part, the turbine output capacity is calculated as Equation (1)[20,36,39].

$$P = F_d u = \frac{1}{2}\rho A(v_{air} - u_{turbine})^2 C_D u_{turbine} \quad (1)$$

And maximum power factor in the blade tip speed ratio (TSR) 1/3:

$$C_P = \frac{P}{\frac{1}{2}\rho A v^3} = C_D \frac{4}{27} \quad (2)$$

By comparing the maximum output power of the drag-type turbine with the Betz limit, the inherent weakness of the efficiency of the drag-type turbines is revealed. Even if we use the maximum drag coefficient, which belongs to the wind-facing hemisphere ($C_D = 1.3$), the maximum output power coefficient is 0.193, much lower than the Betz limit. Another disadvantage of drag turbines is the efficient use of half of the space occupied by the rotor. Although wind technology begins with drag-type mills, in practice, these inherent flaws have hindered the development of more advanced species[40,41].

2.3. Lift-type VAWTs

The turbine was invented in 1931 by Jean Marie Darrieus, a French engineer[21]. HWAT is of lift type, which means that, unlike the Savonius turbine, the lift force causes the turbine to rotate, and the drag force has a deterrent effect (**Figure 1**). The rotation speed of the Darrieus turbine is many times faster than the wind speed it blows. Therefore, the output torque of this turbine is low, and its rotation speed is high. Theoretically, this turbine has the same efficiency as commercial wind turbines. Considering the structure's design limitations and resistance, achieving its efficiency takes work. With lift force, the blade can move faster than the wind, thus producing more power[42,43]. The ratio of the blade tip to wind speed is a comparative indicator for wind turbines. This ratio is approximately 7 for turbine blades with maximum lift power and 0.3 for blades with pressure drag[44–46]. **Figure 2** shows a comparison between turbine efficiencies.

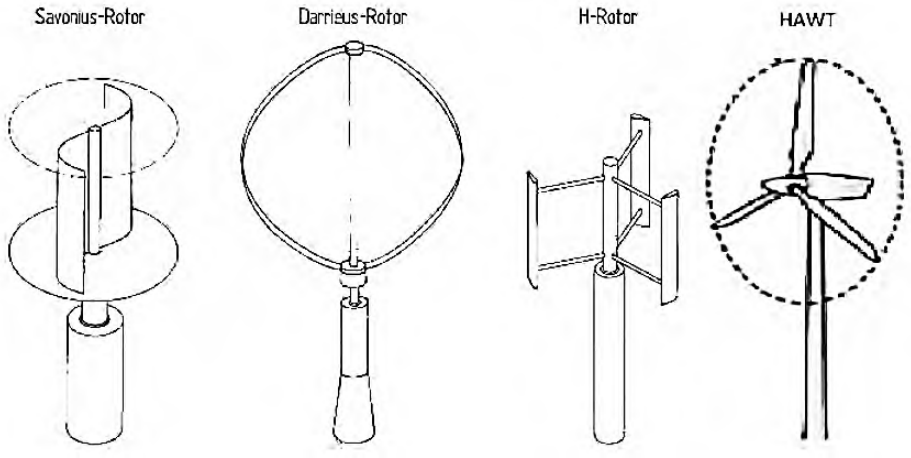

Figure 1. Different types of conventional commercial VAWTs[47].

When the airfoil moves in a circular path, it changes the relative speed of the wind relative to the airfoil, which ultimately produces a variable angle of attack (AOA). This wind movement on the airfoil produces lift force and, thus, torque. When the airfoil rotates around the main axis and passes through the opposite point, the AOA of the airfoil becomes negative. Thus the airfoil production force continues to produce torque by the direction of rotation[48,49].

In this rotor, the AOA with rotation is constantly changing. Therefore, according to the wind direction, maximum AOA and, consequently, most torque is produced in the front and back of the device. These pulsed torques make the design process complicated. At some rotational speeds, the natural frequency of the blades equals this frequency, which causes resonance and destruction of the device. Therefore, in design, these modes should be considered[48,49].

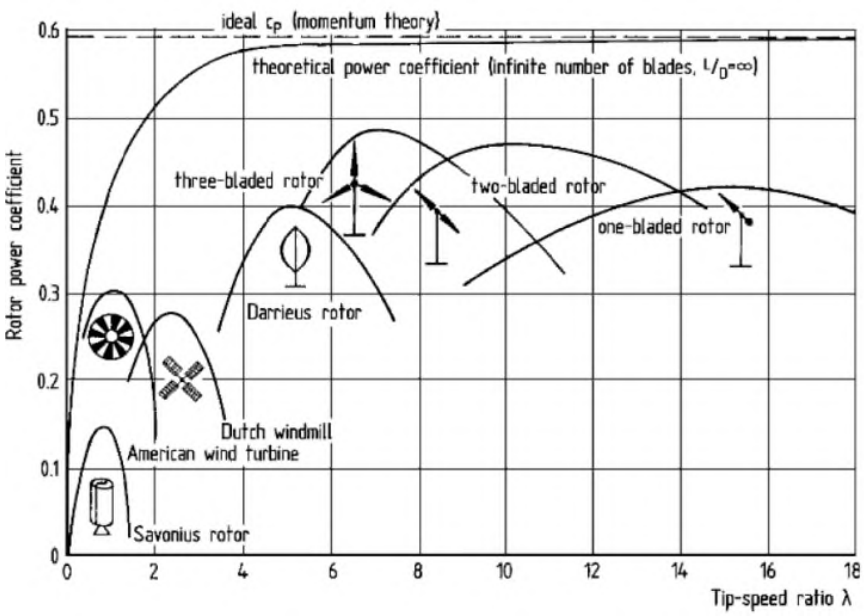

Figure 2. Comparison of the power factor of different wind turbine.

Unlike HAWTs, most of the weight of the blade structure is in the wheel bowl; in this rotor, most weight is located at the end of the arms[50,51]. Therefore, in this mechanism, large centrifugal forces are generated; consequently, many stresses are applied to the structure, which increases the complexity of the design. One of the initiatives to reduce force is rotating wings similar to the egg weight (also named troponin) so that the blades are attached directly to the base[52–54]. The rotating blades compress the column, secured from above with retaining wires. Although the Darrieus rotor is far more practical than the Savonius rotor, it still needs to catch up to horizontal axis turbines in terms of benefits and costs. **Table 1** compares the mentioned rotors[23,55].

Table 1. Comparison of advantages and disadvantages of turbines.

Cases	HAWT	Darrieus	Savonius	References
The shape of the blade	Complicated	Simple	Simple	[23,56]
Rectifier mechanism	Needs	Needless	Needless	[57]
Ability to change the angle of the blade	Yes	Yes	No	[58]
Large-scale construction	Yes	Yes	No	[59]
Rotor weight bearing	Medium	Low	High	[60]
Noise	High	Low	Low	[59,61]
Generator and gearbox location	Top of the tower	Ground	Ground	[62]
Auto start	Yes	Weak	Yes	[16,23]
Foundation	Complicated	Simple	Simple	[23]
Ideal power factor	High	High	Low	[63]

Table 1. (*Continued*).

Cases	HAWT	Darrieus	Savonius	References
Maintenance costs	High	Low	Low	[63–65]
Research done	Much	Little	Little	[23,55]
Structure set	Complicated	Simple	Simple	[66–68]
Dense placing in wind farms	-	-	-	[69,70]
Turbulence influence on wind energy extraction for a medium size vertical axis wind turbine	-	-	-	[71,72]

3. Aerodynamic solution methods

Although the flat-blade Darrieus turbine is one of the simplest types of wind turbines, its aerodynamic study is complicated[73]. Before comparing the existing designs for aerodynamic study, the equations used in these studies are introduced. The flow velocity is not constant upstream and downstream (**Figure 3**). The component of cord velocity and normal velocity is obtained as follows[74,75].

$$V_c = R\omega + V_a cos\theta \tag{3}$$

$$V_n = V_a sin\theta \tag{4}$$

V_a is the axial induction velocity that passes through the rotor, angular velocity, and the rotor placement angle. According to **Figure 2**, the AOA can be calculated from the following equation[76,77].

$$a = tan^{-1}\frac{V_n}{V_c} = tan^{-1}\frac{sin\,\theta}{\frac{R\omega}{V_\infty}/\frac{V_a}{V_\infty} + cos\,\theta} \tag{5}$$

Also, the relative velocity on the blade is obtained as follows.

$$\frac{W}{V_\infty} = \frac{W}{V_a}\times\frac{V_a}{V_\infty} = \frac{V_a}{V_\infty}\sqrt{\left[\left(\frac{R\omega}{V_\infty}\Big/\frac{V_{au}}{V_\infty}\right) + \cos\theta\right]^2 + sin^2\theta} \tag{6}$$

The direction of lift and drag force, its radial and angular components, and the force coefficients in the angular and radial direction shown in **Figure 3** are calculated as follows from the lift and drag coefficients obtained from the laboratory result[78].

$$C_t = C_l \sin\alpha - C_d \cos\alpha \tag{7}$$

$$F_t = \frac{1}{2}C_t\rho CHW^2 \tag{8}$$

Given that Equation (6) is written in terms of position, then the mean angular force can be defined as follows.

$$F_{ta} = \frac{1}{2\pi}\int_0^{2\pi} F_t(\theta)\,d\theta \tag{9}$$

And the output power is obtained as follows.

$$P = F_{ta}RN\omega \tag{10}$$

In the past, several mathematical models based on several theories have been used to predict the performance and design of the Darrieus turbine in various studies. According to research conducted by Islam[79], the most and best-validated models are divided into three categories:

- Momentum models (BEM)

- Vortex model
- Cascade model

Of course, only some of these three models will meet all the critical performance metrics.

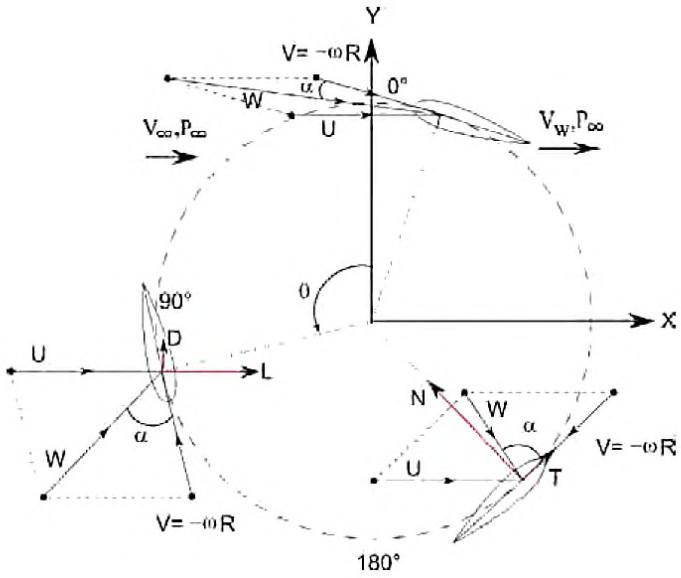

Figure 3. Velocities and forces on the Darrieus rotor[78].

3.1. Momentum models (BEM)

These models have been introduced in different ways. However, the basis of these models is that by placing aerodynamic forces in the direction of flow with momentum changes, the induced speed during flow will be obtained. The most critical problem of these models is that they need to give a good answer for high TSR and solidity because solving momentum equations alone is not enough[79]. In 1974, Templin[80] introduced the single stream tube (SST) model, which was the first and most straightforward. This model was first registered for the windmill but later expanded to the Darrieus turbine. In this theory, it is assumed that the induced velocity is constant along with the rotor and obtained from the drag force's equality along with the flow by momentum change in this direction[81].

This theory pays attention to the effect of airfoil failure[82]. Thus, the effect of geometric variables such as solidity and aspect ratio, as well as the effect of zero lift-drag coefficients, are considered qualitative features in this theory. However, the sheer effects of wind in this model are not considered[79].

Gluert's actuator disk theory[79], states that the uniform velocity passing through the rotor equals the average velocity upstream and downstream (**Figure 4a**). This model does all calculations for a blade that equates the chord length of this blade to the sum of blade lengths. The drag force in the flow direction is the result of momentum change in this direction, and by defining the rotor drag coefficient in Equation (10), we have:

$$F_D = m(V_\infty - V_w) \tag{11}$$

$$C_{DD} = \frac{4(V_\infty - V_a)}{V_a} \tag{12}$$

$$\frac{V_a}{V_\infty} = \left(\frac{1}{1 + {C_{DD}}/{4}} \right) \tag{13}$$

The total torque for the turbine will be obtained from Equations (4)–(9) by placing $\frac{V_a}{V_\infty}$ in Equation (13) during an iterative process. This model can calculate the overall efficiency for the low-load mode. However, according to Wilson's results, it consistently achieves more output power than the laboratory results because the velocity on the downstream and upstream are assumed to be the same. This difference in results increases with increasing solidity and increasing TSR[79].

In 1947, Wilson[83] introduced the multiple stream tube (MST) models. In this model, the volume swept by the turbine is divided into several stream tubes side by side[84]. The aerodynamic dependence of the parallel stream tubes is shown in **Figure 4b**. Previous equations are written for each stream tube. In this model, the changes induced velocity in front of the disk are considered in vertical and horizontal directions. Thus, this model also includes wind shear effects[54,79,85]. Wilson recommended the equation for calculating induced velocity as Equation (14), considering only the lift force[86].

$$\frac{V_a}{V_\infty} = 1 - \left(\frac{k}{2} \times \frac{NC}{R} \times \frac{R\omega}{V_\infty} \times \sin\theta\right) \tag{14}$$

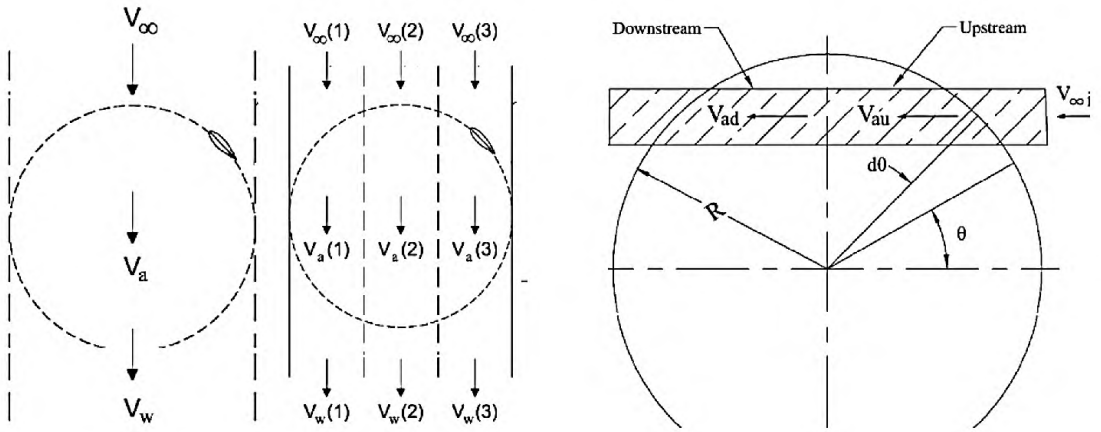

Figure 4. (a) SST model; **(b)** MST model; **(c)** DMST model[79].

In 1981, Paraschivoiu[87,88] introduced the double-multiple streamtube (DMST) model. In this model, calculations are obtained for the two upstream and downstream sections according to **Figure 4c**. The flow of air passing through the tube passes through two actuator disks in a row.

$$V_{au} = uV_\infty \tag{15}$$

$$V_e = (2u - 1)V_\infty \tag{16}$$

$$V_{ad} = u'(2u - 1)V_\infty \tag{17}$$

In which, V_{au} and V_{ad} are induced velocity in upstream and downstream side and, V_e in the wake velocity. Also, u is the induction coefficient in the upstream, and u' is the induction coefficient in the downstream and is always $u' < u$. The turbine's overall drag force in the direction of the stream is obtained from the following equation.

$$F_D = \frac{\sigma}{2\pi} \int_{-\frac{\pi}{2}}^{\frac{\pi}{2}} \frac{W^2}{V_\infty} \left(C_N \frac{cos\theta}{|cos\theta|} - C_T \frac{sin\theta}{|cos\theta|}\right) d\theta \tag{18}$$

This method solved one of Wilson's problems: the equality of the induction velocities of the front and rear blades. However, problems with convergence (especially downstream and high TSR) appeared[79].

The results of these methods showed (**Figures 5** and **6**) as the TSR increases, the turbine power coefficient increases to reach an optimal TSR. After this, the power factor will decrease with increasing TSR. Paraschivoiu also studied the effect of solidity, as shown in **Figure 7**. His results showed that with increasing solidity, the power coefficient in TSR reaches its optimal value.

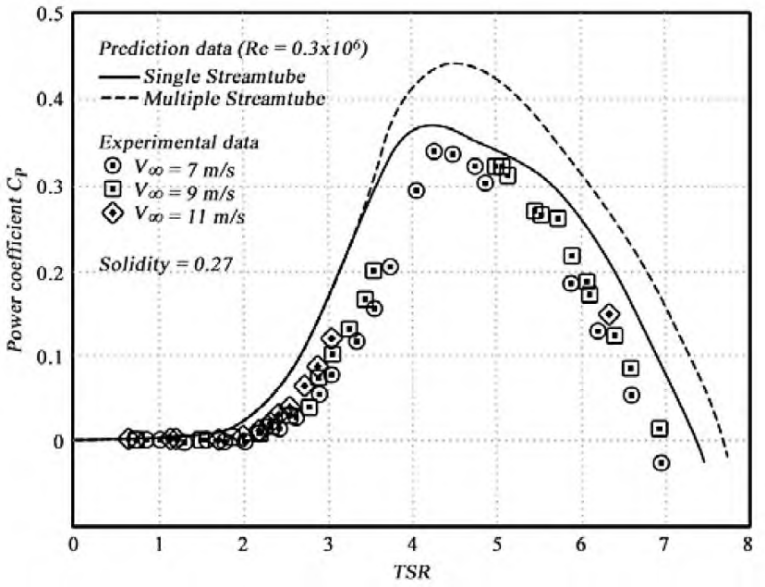

Figure 5. Comparison of SST and MST models with laboratory information[89].

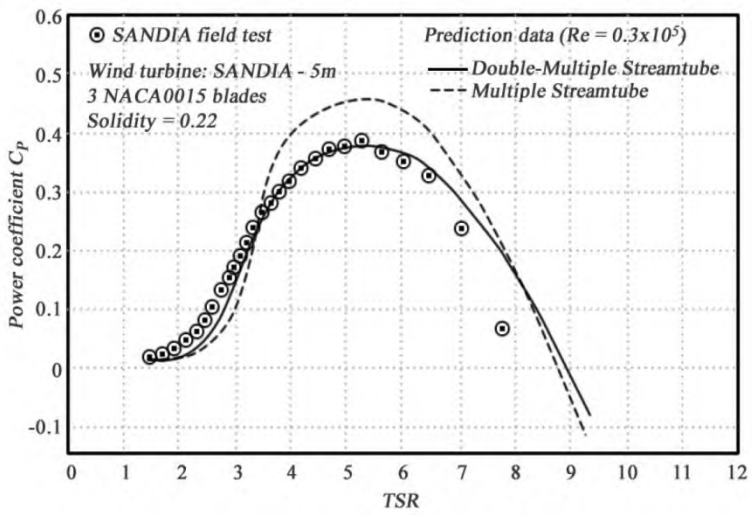

Figure 6. Comparison of multiple and DMST models with laboratory information[89].

In 2013, Batista et al.[89] compared the models as shown in **Figures 5** and **6**. His results showed that the DMST model has the closest adaptation of the three models to laboratory information but also has the most challenging convergence conditions. All three models at higher solidity and higher TSR predict higher results from laboratory data. With the help of these methods, it was possible to obtain the main aerodynamic properties with low calculations. However, these methods, which were unable to model the shape of the flow, cannot investigate the causes of phenomena such as power factor reduction for TSR greater than 6. Another problem with these methods is the need for more accurate airfoil information at attack angles above the stall state.

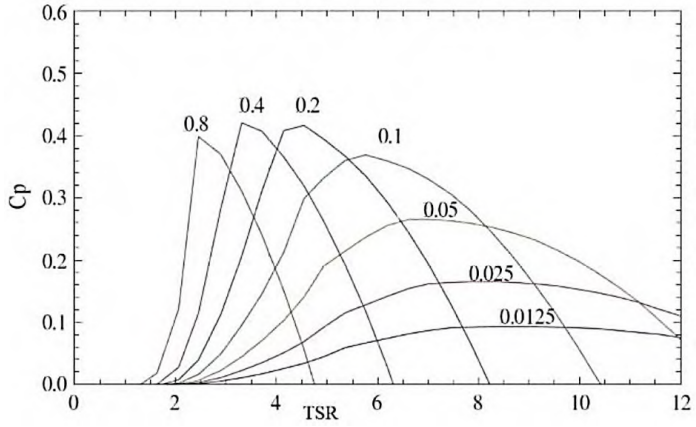

Figure 7. Turbine power coefficient curve in terms of TSR for $\sigma = 0.8$[90].

3.2. Vortex model

The vortex model is based on potential flow. This model calculates the velocity field around the turbine through the influence of velocity in the wake of models. Turbine blades are expressed as concentrated vortexes. The strength of these vortexes is obtained by collecting airfoil coefficient data and calculating the relative flow and AOA. In VAWTs, the blade element is replaced by a substitution vortex filament or a lift line[79]. This method is well compatible with laboratory information and solves some of the problems of the previous method. Dixon's results[91] could explain that as the blade speed increases, less energy is wasted from the wind. However, after exceeding six times the wind speed, the blade collides with the non-renewed wind flow, which reduces the power factor (**Figure 8**). However, this method cannot visualize the flow well and requires many calculations[79,92].

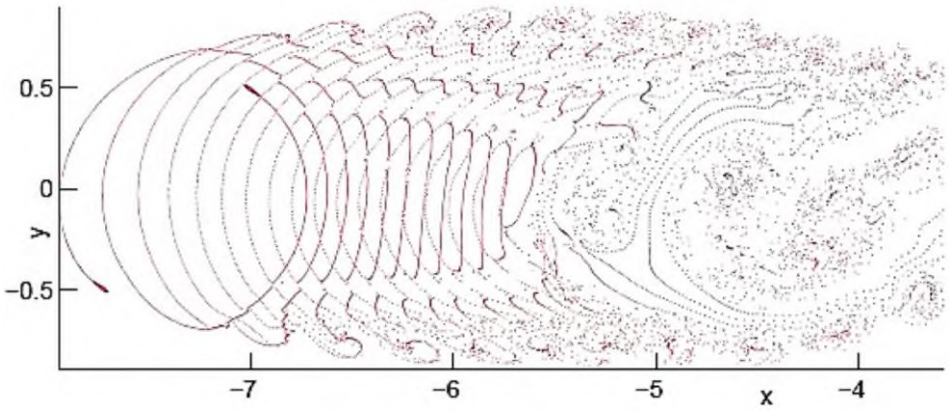

Figure 8. Displays the rise motion of the vortex method[91].

3.3. Vortex model

The periodic equidistant arrangement of several blades or vanes of turbomachinaries is called a cascade. Hence, the cascade is the basic element of the turbomachine, and cascade flow is the essential physical phenomenon for the operation of the machine[93]. The Cascade model was proposed by Hirsch and Mandal to apply the cascade principles, widely used for turbomachinaries, for the analysis of VAWTs for the first time. In this model, the blade airfoils of a turbine are assumed to be positioned in a plane surface (termed as the cascade) with the blade interspace equal to the turbine circumferential distance divided by the number of blades[94].

4. Flow field visualization by particle image velocimetry (PIV)

Aerodynamic models, no matter how well they predict the power and performance coefficients of the turbine, Aerodynamic models are still unable to visualize the flow field. Visualization of the flow field around the wind turbine facilitates the understanding and analysis of the aerodynamic behavior of the wind turbine, which is necessary to improve the efficiency and proper design of the device[95].

In 1999, Fujisawa et al.[96] visualized the flow field in an area of the Darrieus rotor during a dynamic stall by injecting dye. The dye was injected into the fluid stream in this method, and the flow model was observed through the dye path. They used the PIV and regional imaging techniques to measure the blade's average velocity distribution.

In PIV, tracer particles with a specific gravity close to the fluid flow are injected into the fluid without affecting its velocity[97]. These particles move at the same local velocity as the fluid. Images of moving particles are taken at any given moment with the help of a digital camera. Then these images are analyzed to obtain the velocity of the fluid at that moment. They concluded that the dynamic stall phenomenon occurs due to the flow of two pairs of vortices from the blades as they rotate from the rotor. At low rotor speeds (TSR < 3), the AOA is variable and dynamic stall occurs[95].

In 2014, Danao et al.[98] compared the turbulence models Kϵ and Kω-SST with laboratory results (**Figure 9**). Their results showed that model Kω-SST has a more extraordinary ability to model the flow around the rotor. The model was initially introduced for high-spin currents, but corrections were made to model the flow along the wall over time. Therefore, as previously predicted according to their results, this model is better consistent with the laboratory results around turbomachines, and because it is two equations does not increase the calculations.

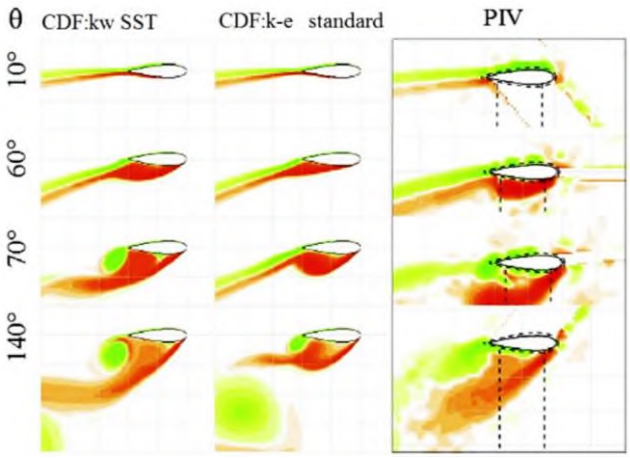

Figure 9. Flow visualization using Kϵ, Kω-SST and PIV[98].

In addition, they examined the effect of wind blowing on a sporadic basis. Their results showed that if the wind enters the turbine in an oscillating manner, the optimal of the blades differs and occurs in less than the steady-state (**Figure 10**).

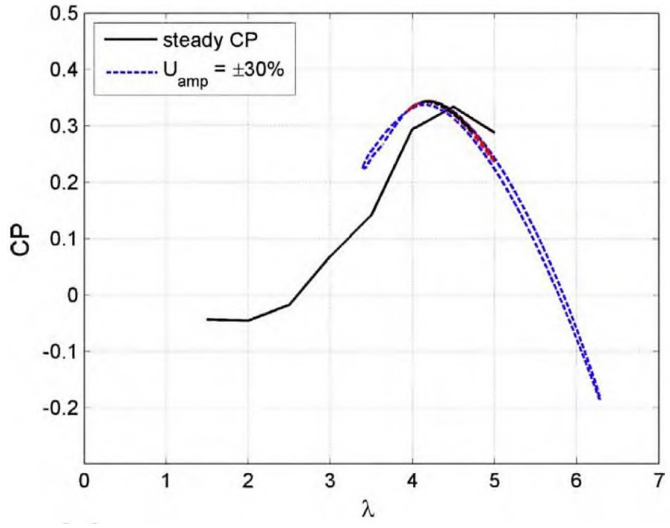

Figure 10. Power factor curve for both steady and oscillating wind modes[98].

5. Computational fluid dynamics (CFD) methods

CFD is now becoming a powerful tool in fluid mechanics that analyzes and solves fluid flow problems using numerical methods and algorithms with the help of electronic computers[99]. Using CFDs can save time and costly testing and can also be used to improve VAWT analysis. A well-tuned CFD model can simulate actual flow conditions that can produce results consistent with laboratory outputs. Therefore, design optimization can be done before entering the construction stage[100–102].

CFD analysis has been widely used to determine power factors in different wind turbine configurations. The CFD technique for visualizing the flow field of a VAWT can be seen in Allet's early work[103]. Debnath et al.[104] used the CFD to test the Savonius-Darrieus rotor, which is more capable of starting than the Darrieus rotor. In 2010, Wang et al.[105] used two unsteady Reynolds-averaged Navier-stokes (URANS) models with standard and Kω-SST to simulate the phenomenon of the dynamic stall at low Reynolds (Re ≈ 105)[106]. After comparing the results of this model with the experimental model, they found that model Kω-SST is better than standard Kω. Model Kω-SST shows the main features of the dynamic stall phenomenon, such as the aerodynamic residual load and the flow structure of the vortexes of the front of the airfoil.

Large eddy simulation (LES) models are more advanced and more powerful than URANS models. They require more computation time, but their results are more accurate. Among the two models, detached eddy simulation (DES) and LES, the DES model is a better model due to the more significant agreement of the results with the experimental results. The DES model combines the LES model and the URANS model. This model not only has a lower computational cost than the LES model but also models the wall area more accurately[107–109]. In testing turbines by the CFD method, the movement of the turbine blades must also be considered in addition to the equations governing the fluid flow field. Turbine motion is generally modeled in three ways: stationary rotor, constant speed rotor, and accelerated rotor[110–112].

5.1. Stationary rotor

In this method, it is assumed that the rotor is fixed, and the resulting current and torque are obtained for several angles of the fluid field. Menet et al.[113] compared the flow field for several angles of the two Savonius turbines. However, they could have obtained better power factor values than the laboratory data. Of course, this method could be more beneficial for lift-type turbines such as Darrieus due to the high importance of the relative speed on the rotor. In 1999, Allet et al.[103] investigated the behavior of an airfoil at

higher angles of the stall for which it did not have adequate laboratory information at rest and combined aerodynamic methods to obtain the power factor for Darrieus turbines. Of course, their data always showed a lower power factor than laboratory data due to the inability of this method to consider dynamic stalls resulting from its static study[110].

5.2. Constant speed rotor

In general, three methods of reference frame method (RFM) and sliding mesh method (SMM), and dynamic mesh are often used to study turbomachines that have moving parts[10,114,115]. The relative coordinate system is adapted to the rotor in the RFM method, which is also the most straightforward method. Instead of the mesh deformation, it is assumed that the boundary conditions are rotating around the axis and that the momentum equations for the rotating device are correct. Of course, this method is not very useful for analyzing turbomachines because it solves the problem steadily and needs to give a better analysis of the problem, which is generally transient[32,116,117].

Korobenko et al.[118] used a complete method known as SMM. In this method, unlike RFM, the mesh shape will change. Amet et al. Divided the solution area into a fixed part and a rotating part in which the rotor was located. For each subdomain, governing equations are solved and related by Equations (19) and (20) through our boundary, known as the interface boundary.

$$U_M - U_S = 0 \tag{19}$$

$$(2\mu\varepsilon U_S - P_S I)n_S + (2\mu\varepsilon U_M - P_M I)n_M = 0 \tag{20}$$

In which I is the unit tensor, S and M are the fixed amplitude and the moving amplitude, respectively, and n are the unit vectors perpendicular to the outside. In this solution, the rotational amplitude equations are given a stationary angular velocity and the forces and torque on the turbine are calculated at each time step. In 2009, Amet et al.[119]. used the same method to investigate the effect of a vortex on the operation of a Darrieus turbine. By defining the reduced frequency as Equation (21), they introduced the ratio of the time of fluid movement on the blade to the time scale of the intensity of changes in the AOA.

$$F^* = \frac{C}{R} \times \frac{1}{\lambda - 1} \times \frac{1}{2\alpha_{max}} \tag{21}$$

For high F^* (greater than 0.05), if the AOA is greater than the static state, the device is prone to strong dynamic failure with vortex separation. **Figure 11** shows two curves, first α in θ for different λ and the other F^* in λ for different solidities. The first curve shows $2 < \lambda < 6$ results in the 9.5 < AOA < 30 degrees. These angles are higher than the 12 for the static stall. For $\lambda > 5$, the AOA does not exceed 12 in the whole half. The second curve shows that a strong dynamic failure is expected if the two conditions >5 and $C/R > 0.1$ are met. Amet compared the separated vortexes for the two AOA 2 and 7. **Figure 12** shows that the pair of vortexes that are clockwise and counter-clockwise detached from the blade when it is upstream and in the downstream part of the rotor may collide with the blade, causing a drop in the blade lift coefficient. Of course, whether this reduction in lift factor reduces the rotor power depends on whether the torque in that area is positive or negative. **Figure 13**, shown for $\lambda = 2$, shows an oscillation drop-in area 8 due to the vortex movement along the stream, which continues in area 15.

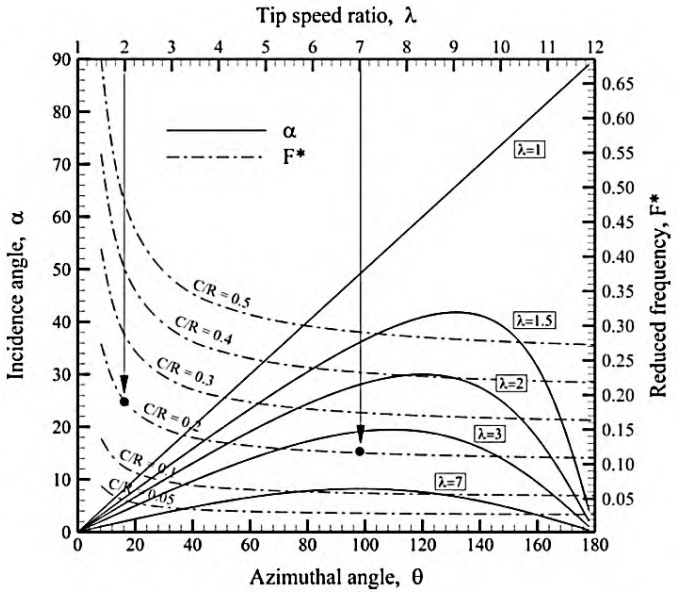

Figure 11. α curve in terms of θ for different λ and F^* in terms of λ for different solidities[119].

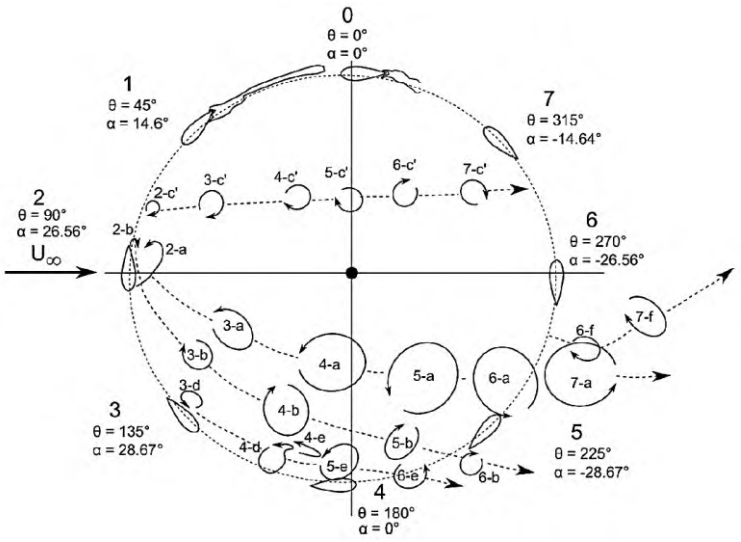

Figure 12. The path of separated vortexes in $\lambda = 2$[119].

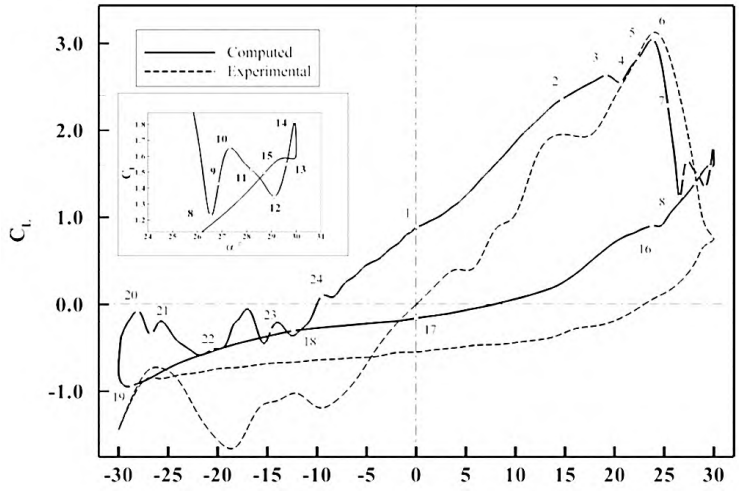

Figure 13. Lift coefficient in a complete revolution in $\lambda = 2$[119].

Figure 14 shows that if the TSR increases, fewer vortexes are formed with lower power and have little effect on the lower blade. **Figure 15** shows the lift factor in a complete rotor rotation in $\lambda = 2$. According to this diagram, with the increase of α, the oscillation caused by the collision of vortexes with the blade is no longer observed. Amet also showed that by increasing the TSR, the flow can not repress the pressure, and the turbine efficiency decreases[119].

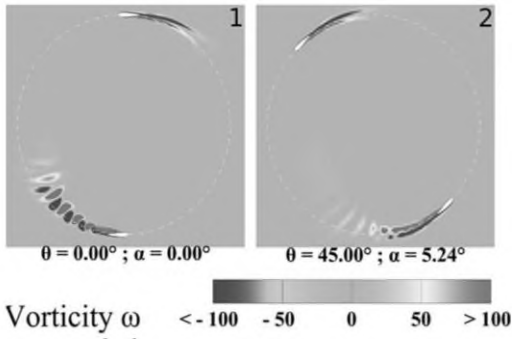

Figure 14. The path of separated vortexes in $\lambda = 7$ [119].

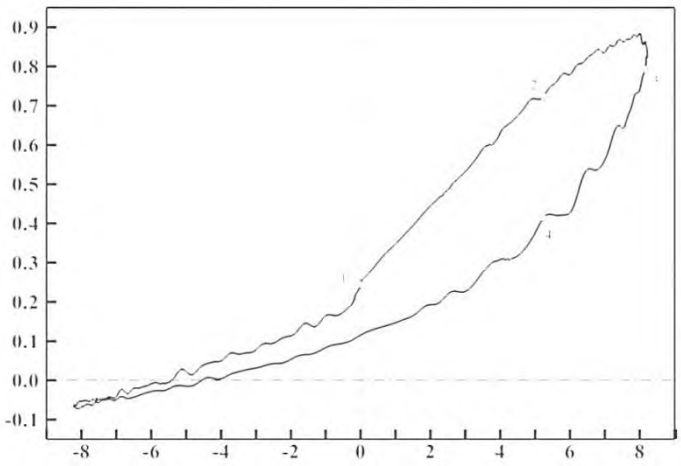

Figure 15. Lift coefficient in a complete revolution in $\lambda = 7$[119].

6. One degree of freedom rotor

According to studies, all the research has been done so far with the constant rotation speed method. Only Alessandro in 2010[120] and Jaohindy in 2013[121] used the accelerated rotation speed for the Darrieus rotor. In this method, the torque applied to the turbine causes proportional acceleration and motion[122]. The rotor motion will be obtained by coupling the Lagrangian equations of CFD and the Euler equations of the rigid body.

Figure 16 shows the dynamic solution flowchart, which consists of three main processes; Solve fluid flow, rotor processing, and mesh deformation processing. In other words, according to this method, the motion of a solid body is coupled by solving the flow field. According to the flowchart, the initial angular velocity is first considered zero. Then the fluid field equations are solved, and the forces acting on the rotor are calculated. In the next step, the angular acceleration will be calculated by the code written according to Equation (22).

$$J_{oz}\ddot{\theta} + M_{oz} \tag{22}$$

$$M_{oz} = M_p + M_\tau + M_f \tag{23}$$

$$M_f = \sum_{K=0}^{H} a_k w^k + M_{gen} \tag{24}$$

J_{oz} is the moment of inertia of the rotor around the z-axis, M_p is the torque due to pressure, M_τ is the torque due to viscous forces, and M_f is the torque generated by the generator load, which also includes mechanical friction[121]. It should be noted that M_τ and M_p are obtained by calculations from the fluid flow field calculated in the previous step and M_p is obtained by Equation (24), whose coefficients are taken into account by the laboratory information[121].

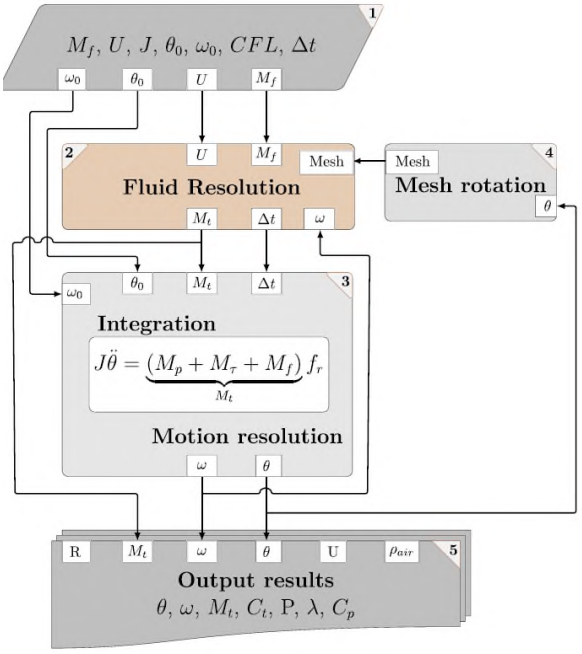

Figure 16. The flowchart is proposed for the dynamic solution method[121].

The acceleration obtained in this step, the new location of the rotor, is determined in the next step. In the next step, the appropriate mesh is deformed with the new location of the rotor by the SMM method[121]. Since the time step is a function of the Courant Friedrichs-Lewy number (CFL) number and the rotation speed of the rotor, it is recommended to change the time step according to the rotor for the appropriate computational volume. Fluent software can calculate the time step in each time step by writing code[116,123,124].

As mentioned, the main weakness of the Darrieus rotor is its initial start. DeCost et al.[125], examining the start of the Darrieus rotor with the PID method, found that the drag forces had a more significant effect on the start of the rotor than the lift force, which may even rotate in the opposite direction. However, after increasing speed and the effects of lift force, the rotor accelerates in the right direction to reach its operating speed. Flow field studies can help obtain optimal starting conditions. Conventional methods that keep the rotor speed constant can certainly not work for this mode, and there is a need for a method that can study the rotor speed based on actual conditions.

In addition to the starting period of the turbine in the rotor operating mode, the speed is not constant even during one rotation. Based on the results of Jaohindy et al.[121], it can be said that after passing the starting period during a rotation, due to the change in torque at different angles, different accelerations are obtained from Equation (22). As a result, we have different angular velocities during a rotation. According to Equation (6), angular velocity strongly affects the relative velocity and lift force, which results in torque with

an oscillating amplitude more significant than the actual state because the rotor speed is obtained from the flow conditions.

7. Conclusion

In this article, wind turbines were first compared. Darrieus turbine, along with many advantages, has a problem of starting and efficiency less than HAWTs, which can be widely used if these problems are solved. The various methods used to evaluate the aerodynamic characteristics of VAWTs were reviewed. Meanwhile, momentum models are cheap but need to be more accurate and suitable for iterative optimization algorithms. The Vertex model has acceptable accuracy but a high computational cost, which has prevented using these models. Of course, with the advances made, these models also have some ability to imagine the flow.

Several aerodynamic models have been analyzed in this paper which are applied for better performance prediction and design analysis of straight-bladed Darrieus-type VAWT. At present the most widely used models are the double-multiple streamtube model, free-Vortex model and the Cascade model. It has been found that, each of these three models has their strengths and weaknesses. Though among these three models, the Vortex models are considered to be the most accurate models according to several researchers, but they are computationally very expensive and in some cases they suffer from convergence problem. It has also been found that the double-multiple streamtube model is not suitable for high tip speed ratios and high-solidity VAWT. On the other hand, the Cascade model gives smooth convergence even in high tip speed ratios and high solidity VAWT with quite reasonable accuracy.

Many CFD studies have been performed on Darrieus turbines that have been able to visualize the flow field well to understand the aerodynamic phenomena around these turbines. Understanding the flow is necessary to optimize the turbine, but most researchers have assumed that the rotor speed is constant. In general rotor research, this simplification does not cause a significant error. However, these models are incapable if special conditions such as the start time of the rotor should be examined. Finally, it is suggested that according to an iterative algorithm, the rotor velocity is obtained as the actual torque reaction.

Supplementary materials

A	Projected frontal area of turbine (m^2)	C	Blade chord (N/m^2)
C_d	Blade drag coefficient	C_D	Turbine overall rotor drag coefficient
C_{DD}	Rotor drag coefficient $F_D/\rho A V_\infty^2$	C_n	Normal force coefficient
C_l	Blade lift coefficient	C_p	Power factor
F_t	Tangential force	F_n	Normal force (in the radial direction)
F_D	Turbine overall drag force	H/C	Aspect ratio
F_{ta}	Average tangential force	H	Height of turbine
F^*	Reduced frequency	P	Power (w)
V	Speed (m/s)	W	Relative speed (m/s)
V_c	Chordal velocity component	V_n	Normal velocity component
V_{au}	Induced velocity in the upstream side	V_{ad}	Induced velocity in the downstream side
u	Induction coefficient in the upstream	u'	Induction coefficient in the downstream

Greek signs

α	AOA (rad)	ρ	Density (kg/m^3)
ω	Angular velocity (rad/s)	σ	Solidity

$\lambda = R\omega/V_\infty$ Tip speed ratio

Subscript

a	Induction	gen	Generator
d	Downstream condition	u	Upstream condition

Conflict of interest

The authors declare no conflict of interest.

Abbreviations

AOA	Angle of Attack
BEM	Momentum Models
CFD	Computational Fluid Dynamics
CFL	Courant-Friedrichs-Lewy Number
DMST	Double Multiple Streamtube
DES	Detached Eddy Simulation
HAWT	Horizontal Axis Wind Turbine
Kω-SST	KΩ-Shear Stress Transport
LES	Large Eddy Simulation
MST	Multiple Streamtube
PIV	Particle Image Velocimetry
RFM	Reference Frame Method
SMM	Sliding Mesh Method
TSR	Tip Speed Ratio
URANS	Unsteady Reynolds-Averaged Navier-Stokes
VAWT	Vertical Axis Wind Turbine

References

1. Amjith L, Bavanish A. A review on biomass and wind as renewable energy for sustainable environment. *Chemosphere* 2022; 293: 133579. doi: 10.1016/j.chemosphere.2022.133579
2. Hao D, Qi L, Tairab AM, et al. Solar energy harvesting technologies for PV self-powered applications: A comprehensive review. *Renewable Energy* 2022; 188: 678–697. doi: 10.1016/j.renene.2022.02.066
3. Cunha RP, Bourne-Webb PJ. A critical review on the current knowledge of geothermal energy piles to sustainably climatize buildings. *Renewable and Sustainable Energy Reviews* 2022; 158: 112072. doi: 10.1016/j.rser.2022.112072
4. Rahman A, Farrok O, Haque MM. Environmental impact of renewable energy source based electrical power plants: Solar, wind, hydroelectric, biomass, geothermal, tidal, ocean, and osmotic. *Renewable and Sustainable Energy Reviews* 2022; 161: 112279. doi: 10.1016/j.rser.2022.112279
5. Machado JTM, Andrés M. Implications of offshore wind energy developments in coastal and maritime tourism and recreation areas: An analytical overview. *Environmental Impact Assessment Review* 2023; 99: 106999. doi: 10.1016/j.eiar.2022.106999

6. Salmerón-Manzano E, Alcayde A, Manzano-Agugliaro F. Renewable energy predictions: Worldwide research trends and future perspective. *Prediction Techniques for Renewable Energy Generation and Load Demand Forecasting* 2023; 93–110.
7. Karmakar SD, Chattopadhyay H. A review of augmentation methods to enhance the performance of vertical axis wind turbine. *Sustainable Energy Technologies and Assessments* 2022; 53: 102469. doi: 10.1016/j.seta.2022.102469
8. Homa M, Pałac A, Żołądek M, et al. Small-scale hybrid and polygeneration renewable energy systems: Energy generation and storage technologies, applications, and analysis methodology. *Energies* 2022; 15(23): 9152. doi: 10.3390/en15239152
9. Pishgar-Komleh S, Keyhani A, Sefeedpari P. Wind speed and power density analysis based on Weibull and Rayleigh distributions (a case study: Firouzkooh county of Iran). *Renewable and Sustainable Energy Reviews* 2015; 42: 313–322. doi: 10.1016/j.rser.2014.10.028
10. Zahedi R, Ghorbani M, Daneshgar S, et al. Potential measurement of Iran's western regional wind energy using GIS. *Journal of Cleaner Production* 2022; 330: 129883. doi: 10.1016/j.jclepro.2021.129883
11. Jahromi S, Moosavian SF, Yaghoubirad M, et al. 4E analysis of the horizontal axis wind turbine with LCA consideration for different climate conditions. *Energy Science & Engineering* 2022; 10(10): 4085–4111. doi: 10.1002/ese3.1272
12. Zahedi R, Ahmadi A, Eskandarpanah R, et al. Evaluation of resources and potential measurement of wind energy to determine the spatial priorities for the construction of wind-driven power plants in damghan city. *International Journal of Sustainable Energy and Environmental Research* 2022; 11(1): 1–22. doi: 10.18488/13.v11i1.2928
13. Alom N, Saha UK. Evolution and progress in the development of savonius wind turbine rotor blade profiles and shapes. *Journal of Solar Energy Engineering* 2019; 141(3): 030801. doi: 10.1115/1.4041848
14. Yang B, Yu T, Shu H, et al. Robust sliding-mode control of wind energy conversion systems for optimal power extraction via nonlinear perturbation observers. *Applied Energy* 2018; 210: 711–723. doi: 10.1016/j.apenergy.2017.08.027
15. Irawan EN, Sitompul S, Yamashita KI, et al. The effect of rotor radius ratio on the performance of hybrid vertical axis wind turbine savonius-darrieus NREL S809. *Journal of Energy and Power Technology* 2023; 5(1): 1–12. doi: 10.21926/jept.2301001
16. Möllerström E, Gipe P, Beurskens J, et al. A historical review of vertical axis wind turbines rated 100 kW and above. *Renewable and Sustainable Energy Reviews* 2019; 105: 1–13. doi: 10.1016/j.rser.2018.12.022
17. Bhutta MMA, Hayat N, Farooq AU, et al. Vertical axis wind turbine—A review of various configurations and design techniques. *Renewable and Sustainable Energy Reviews* 2012; 16(4): 1926–1939. doi: 10.1016/j.rser.2011.12.004
18. Roy S, Das B, Biswas A. A comprehensive review of the application of bio-inspired tubercles on the horizontal axis wind turbine blade. *International Journal of Environmental Science and Technology* 2022; 20(4): 4695–4722.
19. Appadurai M, Fantin Irudaya Raj E, Lurthu Pushparaj T. Sisal fiber-reinforced polymer composite-based small horizontal axis wind turbine suited for urban applications—A numerical study. *Emergent Materials* 2022; 5(2): 565–578.
20. Jha AR. *Wind Turbine Technology*. CRC press; 2010.
21. Spera A. *Wind Turbine Technology*. CRC press; 1994.
22. Wang B, Geoffroy S, Bonhomme M. Urban form study for wind potential development. *Environment and Planning B: Urban Analytics and City Science* 2022; 49(1): 76–91. doi: 10.1177/2399808321994449
23. Al Noman A, Tasneem Z, Sahed MF, et al. Towards next generation savonius wind turbine: Artificial intelligence in blade design trends and framework. *Renewable and Sustainable Energy Reviews* 2022; 168: 112531. doi: 10.1016/j.rser.2022.112531
24. Hesami A, Nikseresht AH, Mohamed MH. Feasibility study of twin-rotor Savonius wind turbine incorporated with a wind-lens. *Ocean Engineering* 2022; 247: 110654. doi: 10.1016/j.oceaneng.2022.110654
25. Estelaji F, Naseri A, Zahedi R. Evaluation of the performance of vital services in urban crisis management. *Advances in Environmental and Engineering Research* 2022; 3(4): 1–19. doi: 10.21926/aeer.2204057
26. Zahedi R, Sadeghitabar E, Ahmadi A. Solar energy potential assessment for electricity generation in the southeastern coast of Iran. *Future Energy* 2023; 2(1): 15–22.
27. Howell R, Qin N, Edwards J, et al. Wind tunnel and numerical study of a small vertical axis wind turbine. *Renewable Energy* 2010; 35(2): 412–422. doi: 10.1016/j.renene.2009.07.025
28. Kumar N, Prakash O. Analysis of wind energy resources from high rise building for micro wind turbine: A review. *Wind Engineering* 2023; 47(1): 190–219. doi: 10.1177/0309524X221118684
29. Trentin PFS, Barros Martinez PHB, Santos GB, et al. Screening analysis and unconstrained optimization of a small-scale vertical axis wind turbine. *Energy* 2022; 240: 122782. doi: 10.1016/j.energy.2021.122782
30. Zemamou M, Aggour M, Toumi A. Review of savonius wind turbine design and performance. *Energy Procedia* 2017; 141: 383–388. doi: 10.1016/j.egypro.2017.11.047

31. Gipe P, Möllerström E. An overview of the history of wind turbine development: Part I—The early wind turbines until the 1960s. *Wind Engineering* 2022; 46(6): 1973–2004. doi: 10.1177/0309524X221117825
32. Manatbayev R, Baizhuma Z, Bolegenova S, et al. Numerical simulations on static Vertical Axis Wind Turbine blade icing. *Renewable Energy* 2021; 170: 997–1007. doi: 10.1016/j.renene.2021.02.023
33. Guo W, Shen H, Li Y, et al. Wind tunnel tests of the rime icing characteristics of a straight-bladed vertical axis wind turbine. *Renewable Energy* 2021; 179: 116–132. doi: 10.1016/j.renene.2021.07.033
34. Song J, Chen J, Wu Y, et al. Topology optimization-driven design for offshore composite wind turbine blades. *Journal of Marine Science and Engineering* 2022; 10(10): 1487. doi: 10.3390/jmse10101487
35. Hand B, Cashman A. A review on the historical development of the lift-type vertical axis wind turbine: From onshore to offshore floating application. *Sustainable Energy Technologies and Assessments* 2020; 38: 100646. doi: 10.1016/j.seta.2020.100646
36. Kim S, Cheong C. Development of low-noise drag-type vertical wind turbines. *Renewable Energy* 2015; 79: 199–208. doi: 10.1016/j.renene.2014.09.047
37. Jiang Y, Liu S, Zao P, et al. Experimental evaluation of a tree-shaped quad-rotor wind turbine on power output controllability and survival shutdown capability. *Applied Energy* 2022; 309: 118350. doi: 10.1016/j.apenergy.2021.118350
38. Zahedi R, Rad AB. Numerical and experimental simulation of gas-liquid two-phase flow in 90-degree elbow. *Alexandria Engineering Journal* 2021; 61(3): 2536–2550. doi: 10.1016/j.aej.2021.07.011
39. Zheng M, Li Y, Teng H, et al. Effect of blade number on performance of drag type vertical axis wind turbine. *Applied Solar Energy* 2016; 52(4): 315–320.
40. Barnes A, Marshall-Cross D, Hughes BR. Towards a standard approach for future Vertical Axis Wind Turbine aerodynamics research and development. *Renewable and Sustainable Energy Reviews* 2021; 148: 111221. doi: 10.1016/j.rser.2021.111221
41. El-Baz AR, Youssef K, Mohamed MH. Innovative improvement of a drag wind turbine performance. *Renewable Energy* 2016; 86: 89–98. doi: 10.1016/j.renene.2015.07.102
42. Saat AF, Rosly N. Aerodynamic analysis of vertical axis wind turbine. *Journal of Aviation and Aerospace Technology* 2019; 1(1).
43. Kaustubhasai N, Balachandra TC. Design and fabrication of hybrid system for highway power generation. In: *Advances in Renewable Energy and Electric Vehicles: Select Proceedings of AREEV 2020.* Springer Singapore; 2022.
44. Wong KH, Chong WT, Sukiman L, et al. Performance enhancements on vertical axis wind turbines using flow augmentation systems: A review. *Renewable and Sustainable Energy Reviews* 2017; 73: 904–921. doi: 10.1016/j.rser.2017.01.160
45. Li J, Cao Y, Wu G, et al. Aerodynamic stability of airfoils in lift-type vertical axis wind turbine in steady solver. *Renewable Energy* 2017; 111: 676–687. doi: 10.1016/j.renene.2017.04.057
46. Adnan AIZ, Mohd S, Saad MMM, et al. Aerodynamics analysis of helical wind turbine rotor high speed train. *Journal of Aviation and Aerospace Technology* 2019; 1(2).
47. Saleh A, Feeny BF. Modal analysis of a vertical-axis darrieus wind turbine blade with a troposkein shape, In: *Topics in Modal Analysis & Testing.* Springer International Publishing; 2019. pp. 325–327.
48. Hand B, Kelly G, Cashman A. Aerodynamic design and performance parameters of a lift-type vertical axis wind turbine: A comprehensive review. *Renewable and Sustainable Energy Reviews* 2021; 139: 110699. doi: 10.1016/j.rser.2020.110699
49. Zhao Z, Wang D, Wang T, et al. A review: Approaches for aerodynamic performance improvement of lift-type vertical axis wind turbine. *Sustainable Energy Technologies and Assessments* 2022; 49: 101789. doi: 10.1016/j.seta.2021.101789
50. Daneshgar S, Zahedi R. Optimization of power and heat dual generation cycle of gas microturbines through economic, exergy and environmental analysis by bee algorithm. *Energy Reports* 2022; 8: 1388–1396. doi: 10.1016/j.egyr.2021.12.044
51. Ren F, Wei Z, Zhai X. A review on the integration and optimization of distributed energy systems. *Renewable and Sustainable Energy Reviews* 2022; 162: 112440. doi: 10.1016/j.rser.2022.112440
52. Roy L, Kincaid K, Mahmud R, et al. Double-multiple streamtube analysis of a flexible vertical axis wind turbine. *Fluids* 2021; 6(3): 118. doi: 10.3390/fluids6030118
53. Koca K, Genç MS, Ertürk S. Impact of local flexible membrane on power efficiency stability at wind turbine blade. *Renewable Energy* 2022; 197: 1163–1173. doi: 10.1016/j.renene.2022.08.038
54. Zahedi R, Daneshgar S, Seraji MAN, et al. Modeling and interpretation of geomagnetic data related to geothermal sources, Northwest of Delijan. *Renewable Energy* 2022; 196: 444–450. doi: 10.1016/j.renene.2022.07.004
55. Chen J, Yang H, Yang M, et al. A comprehensive review of the theoretical approaches for the airfoil design of lift-type vertical axis wind turbine. *Renewable and Sustainable Energy Reviews* 2015; 51: 1709–1720. doi: 10.1016/j.rser.2015.07.065

56. Alom N, Saha UK. Evolution and progress in the development of savonius wind turbine rotor blade profiles and shapes. *Journal of Solar Energy Engineering* 2019; 141(3): 030801. doi: 10.1115/1.4041848
57. Freitas TRS, Menegáz PJM, Simonetti DSL. Rectifier topologies for permanent magnet synchronous generator on wind energy conversion systems: A review. *Renewable and Sustainable Energy Reviews* 2016; 54: 1334–1344. doi: 10.1016/j.rser.2015.10.112
58. Apsley DD, Stansby PK. Unsteady thrust on an oscillating wind turbine: Comparison of blade-element momentum theory with actuator-line CFD. *Journal of Fluids and Structures* 2020; 98: 103141. doi: 10.1016/j.jfluidstructs.2020.103141
59. Ottermo F, Bernhoff H. An upper size of vertical axis wind turbines. *Wind Energy* 2014; 17(10): 1623–1629. doi: 10.1002/we.1655
60. Roga S, Bardhan S, Kumar Y, et al. Recent technology and challenges of wind energy generation: A review. *Sustainable Energy Technologies and Assessments* 2022; 52: 102239. doi: 10.1016/j.seta.2022.102239
61. Ottermo F, Möllerström E, Nordborg A, et al. Location of aerodynamic noise sources from a 200 kW vertical-axis wind turbine. *Journal of Sound and Vibration* 2017; 400: 154–166. doi: 10.1016/j.jsv.2017.03.033
62. Dhanola A, Garg HC. Tribological challenges and advancements in wind turbine bearings: A review. *Engineering Failure Analysis* 2020; 118: 104885. doi: 10.1016/j.engfailanal.2020.104885
63. Wang Y, Hu Q, Li L, et al. Approaches to wind power curve modeling: A review and discussion. *Renewable and Sustainable Energy Reviews* 2019; 116: 109422. doi: 10.1016/j.rser.2019.109422
64. Dao C, Kazemtabrizi B, Crabtree C. Wind turbine reliability data review and impacts on levelised cost of energy. *Wind Energy* 2019; 22(12): 1848–1871. doi: 10.1002/we.2404
65. Tusar MIH, Sarker BR. Maintenance cost minimization models for offshore wind farms: A systematic and critical review. *International Journal of Energy Research* 2022; 46(4): 3739–3765. doi: 10.1002/er.7425
66. Wang L, Kolios A, Liu X, et al. Reliability of offshore wind turbine support structures: A state-of-the-art review. *Renewable and Sustainable Energy Reviews* 2022; 161: 112250. doi: 10.1016/j.rser.2022.112250
67. Civera M, Surace C. Non-destructive techniques for the condition and structural health monitoring of wind turbines: A literature review of the last 20 years. *Sensors* 2022; 22(4): 1627. doi: 10.3390/s22041627
68. Hines EM, Baxter CDP, Ciochetto D, et al. Structural instrumentation and monitoring of the Block Island Offshore Wind Farm. *Renewable Energy* 2023; 202: 1032–1045. doi: 10.1016/j.renene.2022.11.115
69. Dabiri JO. Potential order-of-magnitude enhancement of wind farm power density via counter-rotating vertical-axis wind turbine arrays. *Journal of Renewable and Sustainable Energy* 2011; 3(4): 043104. doi: 10.1063/1.3608170
70. Hou P, Zhu J, Ma K, et al. A review of offshore wind farm layout optimization and electrical system design methods. *Journal of Modern Power Systems and Clean Energy* 2019; 7(5): 975–986. doi: 10.1007/s40565-019-0550-5
71. Molina AC, Troyer T, Massai T, et al. Effect of turbulence on the performance of VAWTs: An experimental study in two different wind tunnels. *Journal of Wind Engineering and Industrial Aerodynamics* 2019; 193: 103969. doi: 10.1016/j.jweia.2019.103969
72. Möllerström E, Ottermo F, Goude A, et al. Turbulence influence on wind energy extraction for a medium size vertical axis wind turbine. *Wind Energy* 2016; 19(11): 1963–1973. doi: 10.1002/we.1962
73. Zahedi R, Ahmadi A, Gitifar S. Feasibility study of biodiesel production from oilseeds in Tehran province. *Journal of Renewable and New Energy* 2023; 10(1): 86–96. doi: 10.52547/JRENEW.10.1.86
74. Loth JL. Aerodynamic tower shake force analysis for VAWT. *Journal of Solar Energy Engineering* 1985; 107(1): 45–49. doi: 10.1115/1.3267652
75. Moghimi M, Motawej H. Developed DMST model for performance analysis and parametric evaluation of Gorlov vertical axis wind turbines. *Sustainable Energy Technologies and Assessments* 2020; 37: 100616. doi: 10.1016/j.seta.2019.100616
76. Wang Z, Wang Y, Zhuang M. Improvement of the aerodynamic performance of vertical axis wind turbines with leading-edge serrations and helical blades using CFD and Taguchi method. *Energy Conversion and Management* 2018; 177: 107–121. doi: 10.1016/j.enconman.2018.09.028
77. Zahedi R, Ghodusinejad MH, Gitifar S. Threats evaluation of border power plants from the perspective of fuel type and providing solutions to deal with them: A case study of Iran. *Transactions of the Indian National Academy of Engineering* 2023; 8(1): 55–67.
78. Homicz GF. VAWT stochastic loads produced by atmospheric turbulence. *Journal of Solar Energy Engineering* 1989; 111(4): 358–366. doi: 10.1115/1.3268335
79. Islam M, Ting DSK, Fartaj A. Aerodynamic models for Darrieus-type straight-bladed vertical axis wind turbines. *Renewable and Sustainable Energy Reviews* 2008; 12(4): 1087–1109. doi: 10.1016/j.rser.2006.10.023
80. Templin RJ. *Aerodynamic Performance Theory for the NRC Vertical-Axis Wind Turbine*. National Aeronautical Establishment; 1974.
81. Hansen M. *Aerodynamics of Wind Turbines*. Routledge; 2015.

82. Daneshgar S, Zahedi R. Investigating the hydropower plants production and profitability using system dynamics approach. *Journal of Energy Storage* 2022; 46: 103919. doi: 10.1016/j.est.2021.103919
83. Wilson RE, Lissaman PBS. Applied aerodynamics of wind power machines. *National Science Foundation* 1974.
84. Asemi H, Daneshgar S, Zahedi R. Experimental investigation of gamma Stirling refrigerator to convert thermal to cooling energy utilizing different gases. *Future Technology* 2023; 2(2): 1–10.
85. Saber E, Afify R, Elgamal H. Performance of SB-VAWT using a modified double multiple stream tube model. *Alexandria Engineering Journal* 2018; 57(4): 3099–3110.
86. Babaie Pirouziana AR, Zahedi R, Ahmadi A, et al. Integration of renewable energy-based systems for transport sector in 2050; A case study in Iran. *Renewable Energy Research and Applications* 2023; 4(1): 21–30. doi: 10.22044/rera.2022.11910.1124
87. Paraschivoiu I. *Double-Multiple Streamtube Model for Darrieus in Turbines. NASA*. Lewis Research Center Wind Turbine Dyn; 1981.
88. Paraschivoiu I. *Wind Turbine Design: With Emphasis on Darrieus Concept*. Presses inter Polytechnique; 2020
89. Batista NC, Melício R, Mendes VMF, et al. Darrieus wind turbine performance prediction: Computational modeling. In: Camarinha-Matos LM, Tomic S, Graça P (editors). *Technological Innovation for the Internet of Things.* Springer Berlin Heidelberg; 2013. pp. 382–391.
90. Mandal A. *Aerodynamics and Design Analysis of Vertical Axis Darrieus Wind Turbines* [Bachelor's thesis]. Vrije Universiteit Brussel; 1986.
91. Dixon K, Simao Ferreira CJ, Hofemann C, et al. A 3D unsteady panel method for vertical axis wind turbines. In: *European Wind Energy Conference & Exhibition EWEC Brussels*. European Wind Energy Association EWEA; 2008. pp. 1–10.
92. Dyachuk E, Goude A. Numerical validation of a vortex model against experimentaldata on a straight-bladed vertical axis wind turbine. *Energies* 2015; 8(10): 11800–11820. doi: 10.3390/en81011800
93. Khah MV, Zahedi R, Mousavi MS, et al. Forecasting renewable energy utilization by Iran's water and wastewater industries. *Utilities Policy* 2023; 82: 101546. doi: 10.1016/j.jup.2023.101546
94. Pourrahmani H, Zahedi R, Daneshgar S, et al. Lab-Scale Investigation of the integrated backup/storage system for wind turbines using alkaline electrolyzer. *Energies* 2023; 16(9): 3761. doi: 10.3390/en16093761
95. Rolin VFC, Porté-Agel F. Experimental investigation of vertical-axis wind-turbine wakes in boundary layer flow. *Renewable Energy* 2018; 118: 1–13. doi: 10.1016/j.renene.2017.10.105
96. Fujisawa N, Takeuchi M. Flow visualization and PIV measurement of flow field around a Darrieus rotor in dynamic stall. *Journal of Visualization* 1999; 1(4): 379–386.
97. Asemi H, Zahedi R, Daneshgar S. Theoretical analysis of the performance and optimization of indirect flat evaporative coolers. *Future Energy* 2023; 2(1): 9–14.
98. Danao LA, Edwards J, Eboibi O, et al. A numerical investigation into the influence of unsteady wind on the performance and aerodynamics of a vertical axis wind turbine. *Applied Energy* 2014; 116: 111–124. doi: 10.1016/j.apenergy.2013.11.045
99. Asemi H, Daneshgar S, Zahedi R. Experimental investigation of gamma Stirling engine coupling to convert thermal to cooling energy in different laboratory conditions. *Resources Environment and Information Engineering* 2022; 4(1): 200–212. doi: 10.25082/REIE.2022.01.004
100. Chowdhury AM, Akimoto H, Hara Y. Comparative CFD analysis of Vertical Axis Wind Turbine in upright and tilted configuration. *Renewable Energy* 2016; 85: 327–337. doi: 10.1016/j.renene.2015.06.037
101. Hassanpour M, Azadani LN. Aerodynamic optimization of the configuration of a pair of vertical axis wind turbines. *Energy Conversion and Management* 2021; 238: 114069. doi: 10.1016/j.enconman.2021.114069
102. Wong KH, Chong WT, Poh SC, et al. 3D CFD simulation and parametric study of a flat plate deflector for vertical axis wind turbine. *Renewable Energy* 2018; 129: 32–55. doi: 10.1016/j.renene.2018.05.085
103. Allet A, Hallé S, Paraschivoiu I. Numerical simulation of dynamic stall around an airfoil in Darrieus motion. *Journal of Solar Energy Engineering* 1999; 121(1): 69–76. doi: 10.1115/1.2888145
104. Debnath BK, Biswas A, Gupta R. Computational fluid dynamics analysis of a combined three-bucket Savonius and three-bladed Darrieus rotor at various overlap conditions. *Journal of Renewable and Sustainable Energy* 2009; 1(3): 033110. doi: 10.1063/1.3152431
105. Wang S, Ingham DB, Ma L, et al. Numerical investigations on dynamic stall of low Reynolds number flow around oscillating airfoils. *Computers & Fluids* 2010; 39(9): 1529–1541. doi: 10.1016/j.compfluid.2010.05.004
106. Khah MV, Asemi H, Daneshgar S, et al. Thermal analysis and optimization of indirect flat evaporative coolers. *International Journal of Thermofluids* 2022; 16: 100246. doi: 10.1016/j.ijft.2022.100246
107. Simão Ferreira C, Van Kuik G, Van Bussel G, et al. Visualization by PIV of dynamic stall on a vertical axis wind turbine. *Experiments in Fluids* 2009; 46(1): 97–108.
108. Lei H, Zhou D, Bao Y, et al. Three-dimensional improved delayed detached eddy simulation of a two-bladed vertical axis wind turbine. *Energy Conversion and Management* 2017; 133: 235–248. doi: 10.1016/j.enconman.2016.11.067

109. Shamsoddin S, Porté-Agel F. A large-eddy simulation study of vertical axis wind turbine wakes in the atmospheric boundary layer. *Energies* 2016; 9(5): 366. doi: 10.3390/en9050366
110. Battisti L, Persico G, Dossena V, et al. Experimental benchmark data for H-shaped and troposkien VAWT architectures. *Renewable Energy* 2018; 125: 425–444. doi: 10.1016/j.renene.2018.02.098
111. Santamaría L, Oro JMF, Díaz KMA, et al. Novel methodology for performance characterization of vertical axis wind turbines (VAWT) prototypes through active driving mode. *Energy Conversion and Management* 2022; 258: 115530. doi: 10.1016/j.enconman.2022.115530
112. Miao W, Liu Q, Zhang Q, et al. Recommendation for strut designs of vertical axis wind turbines: Effects of strut profiles and connecting configurations on the aerodynamic performance. *Energy Conversion and Management* 2023; 276: 116436. doi: 10.1016/j.enconman.2022.116436
113. Menet JL, Bourabaa N. Increase in the Savonius rotors efficiency via a parametric investigation. In: Proceedings of the European Wind Energy Conference & Exhibition; 22–25 November 2004; London, UK. pp. 22–25.
114. Hu B, Nian H, Li M, et al. Impedance characteristic analysis and stability improvement method for DFIG system within PLL bandwidth based on different reference frames. *IEEE Transactions on Industrial Electronics* 2022; 70(1): 532–543. doi: 10.1109/TIE.2022.3150092
115. Siddiqui MS, Khalid MH, Badar AW, et al. Parametric analysis using CFD to study the impact of Geometric and numerical modeling on the performance of a small scale horizontal axis wind turbine. *Energies* 2022; 15(2): 505. doi: 10.3390/en15020505
116. Parakkal JU, El Kadi K, El-Sinawi A, et al. Numerical analysis of VAWT wind turbines: Joukowski vs classical NACA rotor's blades. *Energy Procedia* 2019; 158: 1194–1201. doi: 10.1016/j.egypro.2019.01.306
117. Naccache G, Paraschivoiu M. Parametric study of the dual vertical axis wind turbine using CFD. *Journal of Wind Engineering and Industrial Aerodynamics* 2018; 172: 244–255. doi: 10.1016/j.jweia.2017.11.007
118. Korobenko A, Hsu MC, Akkerman I, et al. Aerodynamic simulation of vertical-axis wind turbines. *Journal of Applied Mechanics* 2014; 81(2): 021011. doi: 10.1115/1.4024415
119. Amet E, Maître T, Pellone C, et al. 2D numerical simulations of blade-vortex interaction in a darrieus turbine. *Journal of Fluids Engineering* 2009; 131(11): 111103. doi: 10.1115/1.4000258
120. D'Alessandro V, Montelpare S, Ricci R, et al. Unsteady Aerodynamics of a Savonius wind rotor: A new computational approach for the simulation of energy performance. *Energy* 2010; 35(8): 3349–3363. doi: 10.1016/j.energy.2010.04.021
121. Jaohindy P, Ennamiri H, Garde F, et al. Numerical investigation of airflow through a Savonius rotor. *Wind Energy* 2014; 17(6): 853–868. doi: 10.1002/we.1601
122. Ghoshchi A, Zahedi R, Pour ZM, et al. Machine learning theory in building energy modeling and optimization: A bibliometric analysis. *International Journal of Green Energy* 2022; 1(4). doi: 10.53964/jmge.2022004
123. Fluent A. *Ansys Fluent 12.0 Theory Guide*. ANSYS Inc; 2009.
124. Rezaeiha A, Kalkman I, Blocken B. CFD simulation of a vertical axis wind turbine operating at a moderate tip speed ratio: Guidelines for minimum domain size and azimuthal increment. *Renewable Energy* 2017; 107: 373–385. doi: 10.1016/j.renene.2017.02.006
125. DeCoste J, Smith A, White D, et al. *Self-starting Darrieus Wind Turbine.* Design Project Mech 4020. Dalhousie University, Canada; 2004.